

# Daily and seasonal dynamics of suspended particles in the Rhône River plume based on remote sensing and field optical measurements

Thomas Lorthiois · David Doxaran · Malik Chami

Received: 15 April 2011 / Accepted: 3 January 2012  
© Springer-Verlag 2012

**Abstract** Satellite ocean colour remote sensing can serve as a powerful tool to assess river plume characteristics because it provides daily mapping of surface suspended particulate matter (SPM) concentration at high spatial resolution. This study's ultimate objective was to better understand daily and seasonal particle dynamics in a coastal area strongly influenced by freshwater discharge and wind—the Rhône River (France), this being the major source of terrestrial input to the Mediterranean Sea. SPM concentrations and biogenic composition (chlorophyll a, organic carbon) were investigated during several bio-optical field campaigns conducted in spring–autumn of 2010 both from aboard a research vessel and by means of an autonomous profiling float. Freshwater discharge and wind velocities varied significantly during the year, associated with marked fluctuations in surface SPM (upper 1 m), even within hours and not restricted to any specific season. Thus, the range was ca. 12–25 g m<sup>-3</sup> (dry mass basis) on 9 April (spring), and ca. 3–39 g m<sup>-3</sup> on 4–5 November (late autumn). Short-term variations were observed also in SPM composition in terms of POC (albeit not chl a), with POC/SPM ratios ranging between ca. 3 and 11% over ca. 3 weeks in spring. Nevertheless, the particulate backscattering coefficient ( $b_{bp}$ ) proved to be a robust proxy of SPM concentration in the river plume ( $b_{bp}(770)=0.0076 \times \text{SPM}$ ,  $R^2=0.80$ ,  $N=56$ ). It has recently been demonstrated that 80% of the Rhône's terrestrial

discharge occurs during flood events. The results of the present study revealed that, under these conditions, SPM is constrained largely within surface waters (i.e. at depths <5 m), with only weak daily vertical variability. By implication, ocean colour satellite data are highly suitable in meaningfully estimating the overall SPM load exported by the Rhône River to the Mediterranean. These findings make a solid contribution to future improvements of three-dimensional sediment transport models for the region and similar settings.

## Introduction

Suspended particles in coastal waters have diverse origins such as river discharge, coastal erosion, resuspension, and aeolian transport, and there exists a wealth of information on the physical, geological and biogeochemical processes controlling the input, transport and fate of terrestrial particles exported by rivers to the ocean (see overviews in Robinson and Brink 2005, and Milliman and Farnsworth 2011). Riverine inputs can be temporally highly variable, encompassing flood events associated with high sediment supply as well as longer periods of low discharge (e.g. Wheatcroft and Borgeld 2000 for the Eel River in northern California, and Antonelli et al. 2008 for the Rhône River, southern France). In the absence of wind forcing, river plumes commonly present strong density interfaces between fresh and saline waters, whereby the freshwater discharged by rivers remains constrained to the upper few metres below the sea surface and can be transported offshore by buoyancy. The ultimate extent and orientation of each plume are controlled largely by interactions between the magnitude of river discharge, wind conditions and regional circulation. Compared to the river itself, turbulence is typically lower within the plume, facilitating flocculation in the presence of saltwater and biogenic material. Terrigenous

Responsible guest editor: O. Mikkelsen

T. Lorthiois (✉) · D. Doxaran · M. Chami  
Laboratoire d'Océanographie de Villefranche,  
Université Pierre et Marie Curie, CNRS, UMR 7093,  
06230 Villefranche-sur-Mer, France  
e-mail: thomas.lorthiois@obs-vlfr.fr

M. Chami  
Institut Universitaire de France,  
103 bd Saint-Michel,  
75005 Paris, France

particles assemble into complex aggregates or flocs composed of mineral matter, organic material and water (Dyer 1986; Eisma et al. 1991). The larger size and mass of flocs increase their settling velocity, which explains why most of the finely dispersed material exported by rivers is commonly deposited in prodeltas close to river mouths.

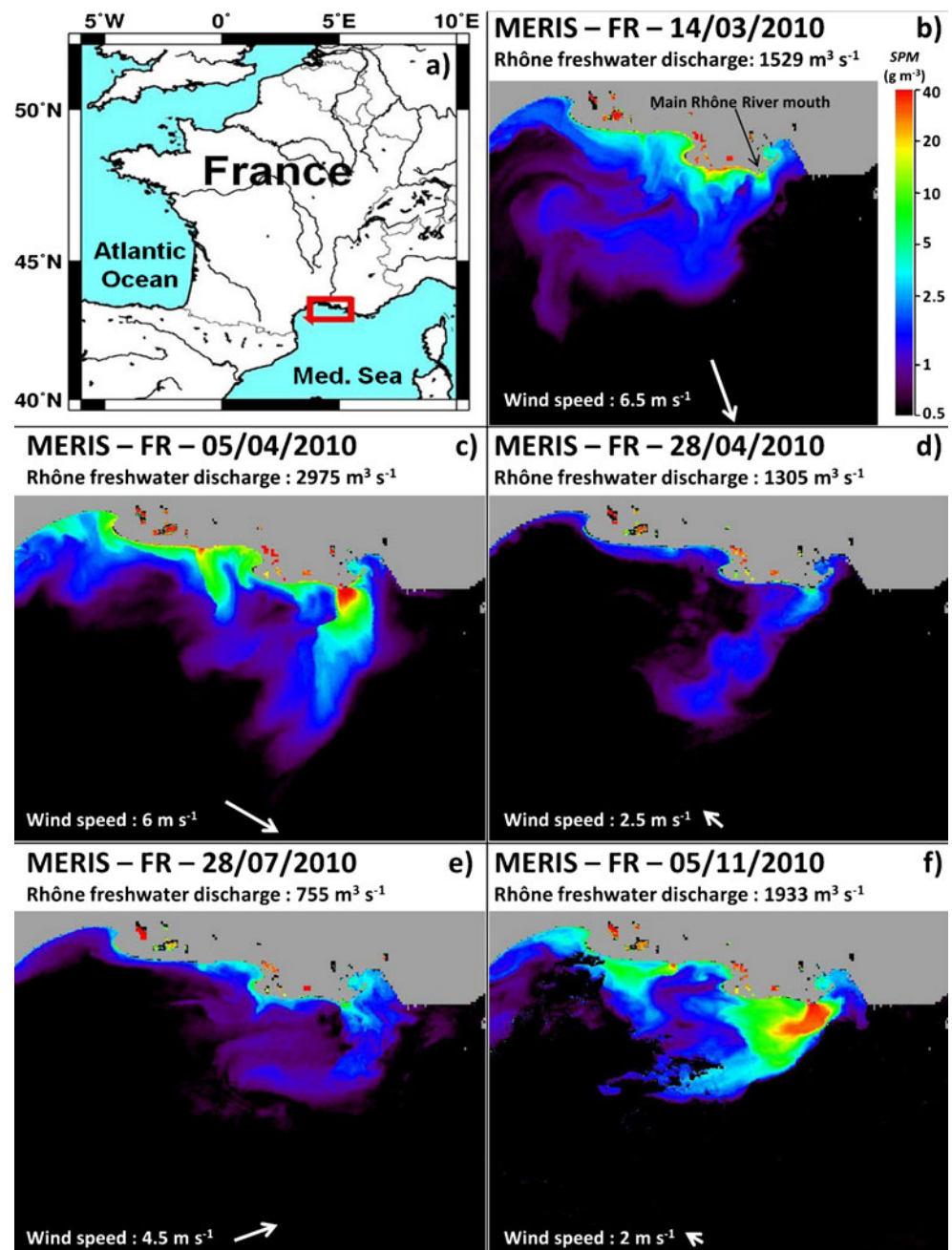
In the present study area, Fig. 1 illustrates the striking dimensions and dynamics of the Rhône River plume in the Gulf of Lion (GoL) in the western Mediterranean Sea, as observed from March to November 2010 by the MERIS full-resolution ocean colour satellite sensor (cf. below). Information provided by satellite remote sensing is strictly limited to

the subsurface layer of turbid coastal waters, and is strongly impaired by cloud cover. On their own, these data evidently do not suffice to perform analyses of the daily dynamics of suspended particles throughout the water column. This requires additional field data of higher temporal and depth resolutions than those offered by satellite observations.

### Existing challenges in SPM assessments

For coastal waters, there is as yet no universally applicable algorithm for quantifying the concentration of suspended

**Fig. 1** a Map of study area. b–f Surface SPM concentrations (dry mass basis) retrieved on 5 days in spring (March, April), summer (July) and late autumn (November) 2010 from full-resolution (FR, 300 m) MERIS satellite data (European Space Agency) by applying the neural network case 2 water algorithm of Doerffer and Schiller (2007), together with Rhône River freshwater discharge, wind speed and direction



particulate matter (SPM, typically in  $\text{g m}^{-3}$ ), this being the main limitation to develop mapping of SPM concentration based on remote sensing (Acker et al. 2005). To interpret remote sensing measurements, in situ data are needed to establish empirical relationships between SPM concentrations and optical parameters. Ouillon et al. (1997) and Forget and Ouillon (1998) performed regression analyses on in situ reflectance and SPM concentration in the Rhône River plume. Applying the derived empirical relationships to SPOT-XS and Landsat-TM images, it was found that measured SPM concentrations were typically 2 times as high as satellite-derived product levels.

In the GoL, MERIS full spatial resolution (300 m) near-daily synoptic maps of SPM concentrations assessed by means of the neural network case 2 water algorithm of Doerffer and Schiller (2007) for selected days in spring, summer and autumn 2010 provide qualitative information on the spatial extent of the Rhône plume under various riverine discharge and wind conditions (Fig. 1). Nevertheless, such data are limited to surface waters. Forget et al. (1999, 2001) studied the sensitivity of water reflectance to variations in SPM concentration with depth. They developed an inversion method for a radiative transfer model restricted to the simple case of a two-layer ocean and tested it on various documented experimental data, also from the Rhône (also see Ouillon 2003). Reasonably good estimates of mean sediment concentration were obtained for the upper but not the lower water column.

Within this context, the first objective of the present study was to document and interpret the in situ daily dynamics of particle concentration gradients within surface waters and deeper in the water column of a coastal area strongly influenced by both riverine discharge and wind activity, using Rhône River data. How relevant is the spot information from one satellite image in terms of SPM variations occurring during a whole day? The second objective was to refine the input parameters of a three-dimensional sediment transport model currently being developed for Rhône River coastal waters. Satellite remote sensing images provide a two-dimensional horizontal synoptic view, whereas in situ vertical profiles would yield additional information for the depth dimension. The third objective was to investigate the seasonal dynamics of suspended particles in terms of their concentration and biogenic composition. For this purpose, bio-optical field measurements were carried out at various seasons during 2010 using (1) an oceanographic research vessel along regular transects from the river mouth to offshore waters and (2) an autonomous bio-optical profiling float deployed in the vicinity of the river mouth.

### Physical setting

The Gulf of Lion comprises one of the largest continental margins in the Mediterranean Sea, and is strongly affected

by the Rhône River in terms of freshwater and solid inputs (e.g. Pont et al. 2002). Indeed, this river is the dominant (80%) source of terrigenous material (Durrieu de Madron et al. 2000) and contributes up to 95% of the freshwater discharge in the GoL (Bourrin and Durrieu de Madron 2006). The Rhône River subdivides into two branches 10 km southwards of the city of Beaucaire, with the main branch channelling 90% of the total freshwater discharge. Highly variable climatic conditions along the drainage basin (one of the largest in Europe) induce a strongly fluctuating freshwater discharge, from commonly less than  $700 \text{ m}^3 \text{ s}^{-1}$  in summer to more than  $4,000 \text{ m}^3 \text{ s}^{-1}$  in spring and autumn (data collected 65 km upstream at Beaucaire by the Compagnie Nationale du Rhône). During the present study period (2010), the values varied from 550 to more than  $4,500 \text{ m}^3 \text{ s}^{-1}$  (Fig. 2). Within the framework of a long-term monitoring programme, in June 2009 a fixed monitoring buoy (the so-called Mesurho) was installed 2 km south-east of the river mouth at a bottom depth of 20 m. It is equipped with subsurface and bottom sensors which continuously record water temperature, salinity, turbidity, and current velocities.

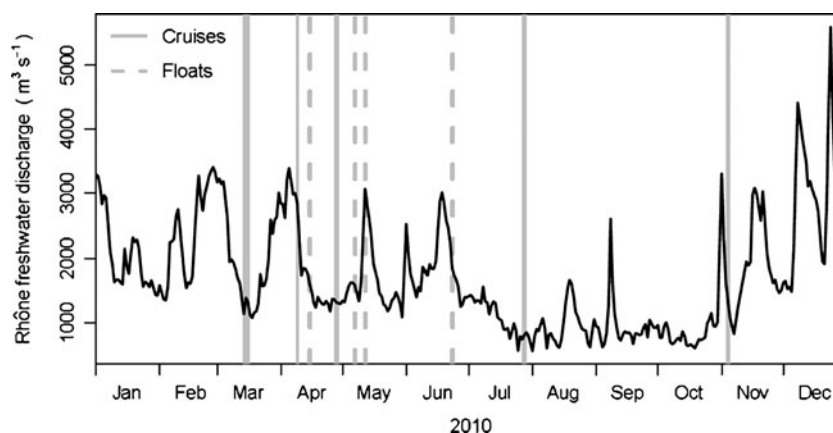
The GoL is influenced by several strongly varying physical processes involving, for example, dense water formation and cascading, upwelling cells, continental winds, and large-scale circulation induced by the northern current along the continental slope (Millot 1990). In contrast, the tidal amplitude is small, typically only a few centimetres. Tidal currents are therefore much weaker than those associated with other processes mentioned above (Lamy et al. 1981). For the Rhône River plume, vertical velocity patterns have been assessed by means of hydrodynamic models by Estournel et al. (2003) and Dufois (2008).

Broche et al. (1998) showed that the plan shapes of the plume (i.e. its extent and orientation) are controlled by wind and river freshwater discharge, commonly associated with its vertical structure changing from a two-layer distribution to a single, thicker mixed layer. Modelling by Estournel et al. (2001) predicted the main characteristics of the plume under varying wind conditions, confirming the pioneer work of Demarcq and Wald (1984). Under a constant NW wind, the plume is pushed offshore; onshore winds cause a larger dispersion and longer residence time of the plume on the continental shelf.

### Materials and methods

Bio-optical field measurements were carried out from on-board the Antédon II research vessel (CNRS/INSU) in the vicinity of the main Rhône River mouth (Fig. 1). Five field campaigns were conducted from spring to autumn 2010 along transects extending from ca. 2 to 7 km offshore the

**Fig. 2** Rhône freshwater discharge recorded in 2010 by the Compagnie Nationale du Rhône at Beaucaire (65 km upstream). *Continuous grey lines* Dates of cruise fieldwork, *dashed grey lines* deployment of the autonomous profiling float



river mouth, these being on 15–17 March (spring, 40 stations), 9 April (12 stations), 28–29 April (24 stations), 28–29 July (summer, 29 stations) and 4–5 November (autumn, 19 stations). Note that the maximum bottom depth sampling of the November cruise was limited to 20 m due to the technical specifications of one of the sensors.

At each station, water samples were collected using Niskin bottles within the surface layer (upper 1 m) and sometimes at ca. 2 m above the bottom. SPM concentration was determined by filtering known volumes ( $V$ , in l) of seawater (0.2 to 2 l, depending on turbidity) in triplicate through precombusted (450°C) and pre-weighed (mass  $M_0$ , in mg) 25 mm glass-fibre filters (Whatman, GF/F 0.7  $\mu\text{m}$  nominal pore size) at low vacuum (Van der Linde 1998). Each filter was then rinsed with Milli-Q water, and stored at  $-20^\circ\text{C}$  on the ship and subsequently at  $-80^\circ\text{C}$  once back at the laboratory onland. At final processing, filters were dried for 24 h at  $60^\circ\text{C}$ , then weighed under a dry atmosphere (mass  $M_1$ , in mg) to obtain:

$$\text{SPM} = (M_1 - M_0)/V \quad (1)$$

Based on triplicate SPM concentration measurements, the mean uncertainty was less than 5%.

Chlorophyll analyses were performed on surface water samples collected during the spring cruises. In each case, a volume  $V$  (0.2 to 2 l) of seawater was filtered as described above and the filters stored at  $-80^\circ\text{C}$  until determination of chlorophyll a concentration (chl a, in  $\text{mg m}^{-3}$ ) by means of high-performance liquid chromatography as described by Ras et al. (2008). The uncertainty on chl a measurements was less than 1%.

Particulate organic carbon (POC) contents were determined on the same GF/F filters as those used for SPM determination. The filters were acidified with 200–350  $\mu\text{l}$  2 N HCl to remove carbonates, and then dried at  $60^\circ\text{C}$  overnight and assayed on a CHN analyzer (Perkin Elmer 2400) with combustion at  $925^\circ\text{C}$ . Mean uncertainty was 11%, based on triplicate measurements.

A frame to which various instruments had been fixed was deployed to measure the following parameters at least every half metre down the water column: (1) water pressure, temperature and salinity, using a Seabird SBE19 CTD sensor, and (2) light backscattering coefficients at several visible and near-infrared wavelengths (cf. below). The remote sensing reflectance signal ( $R_{rs}$ , in  $\text{sr}^{-1}$ ) measured by satellite sensors is a function of two inherent optical properties, namely the total absorption coefficient  $a$  (in  $\text{m}^{-1}$ ) and the total backscattering coefficient  $b_b$  (in  $\text{m}^{-1}$ ; Gordon et al. 1975). Level 2 ocean colour satellite products, such as those obtained using the GSM algorithm (Maritorena et al. 2002) or the neural network case 2 water algorithm (Doerffer and Schiller 2007), enable retrieving the particulate backscattering coefficient ( $b_{bp}$ , in  $\text{m}^{-1}$ ). Note that  $b_{bp}$  is a key parameter because it can be related to suspended matter concentration. Moreover, the light backscattered by water can be used to determine turbidity (e.g. see the widely used optical backscattering sensor, OBS, which measures the near-infrared light backscattered by suspended particles at angles of  $140$ – $165^\circ$ ).

Three ECO-BB3 sensors (Wetlabs Inc.) served to measure the light backscattered by suspended particles at a fixed angle of  $117^\circ$ ,  $\beta(117)$  in  $\text{m}^{-1} \text{sr}^{-1}$ , at the wavelengths 440, 470, 532, 650, 720, 770 and 870 nm.  $\beta$  values were corrected for absorption losses along the photon path lengths using absorption coefficients measured with an ac-9 sensor (Wetlabs Inc.) pre-calibrated with distilled water. Water backscattering at  $117^\circ$ ,  $\beta_w$ , was subtracted from total backscattering to obtain  $\beta_p$ . Finally,  $\beta_p$  was multiplied by a factor  $\chi_p$  to obtain total particulate backscattering ( $b_{bp}$ ):

$$b_{bp}(\lambda) = 2 \times \pi \times \chi_p \times \beta_p(\theta, \lambda) \quad (2)$$

where  $\lambda$  is the wavelength (in nm),  $\theta$  the scattering angle (in degrees) and  $\chi_p$  a factor of value 1.1 assumed to be wavelength-independent (Boss and Pegau 2001). Chami et al. (2006) tested the assumption that  $\chi_p$  is wavelength-independent and found that the particulate backscattering coefficient  $b_{bp}$  would be estimated within  $\pm 10\%$  error.

Uncertainty associated with the absorption correction was less than 1% in the present study.

In addition to the field measurements carried out during the cruises, an autonomous profiling float was deployed twice offshore the Rhône River mouth. This so-called ProvBio float has been developed by IFREMER, NKE Inc. and the Laboratoire d'Océanographie de Villefranche, its design based on the Provor-CTS3 profiling float (Le Reste et al. 2009; Doxaran et al. 2011). It is equipped with a CTD sensor (Seabird 41CP) and several miniaturized optical sensors, including a Wetlabs ECO3 to measure  $b_{bp}$  at 532 nm. The ProvBio profiling float was deployed for the first time in coastal waters in April 2010. It was programmed to perform three vertical profiles of optical measurements during the daytime, successively at 06:00, 12:00 and 18:00 hours local time, and was grounded on the bottom during the night to minimise offshore drifting. After 40 days of deployment, the float had moved seawards up to the limits of the Rhône River plume, due to an extreme spring flood event. It was therefore recovered at the end of May 2010, and then deployed again closer onshore. Since river freshwater discharge decreased substantially after the spring flood events, the float maintained its position in the plume within 20 km of the river mouth during 30 days until recovery. Note that  $b_{bp}$  was not corrected for absorption losses in this case (cf. there is no absorption sensor on the float); however, a sensitivity analysis showed that the absorption correction effect on  $b_{bp}$  can be neglected (about 1%).

Hourly measurements of wind direction and speed are available from Météo France for the Port-de-Bouc meteorological station, 16 km northeast of the Rhône River mouth.

## Results

### Wind conditions

From 9 to 16 March, there was a steady NW wind with an overall speed of  $6 \text{ m s}^{-1}$  and gusts of about  $14 \text{ m s}^{-1}$ . On 17 March, the wind direction became NE and then S from 10:00 to 22:00 hours (local time), with an overall speed of about  $5 \text{ m s}^{-1}$ . On 4–5 April, there was a NW wind of about  $6 \text{ m s}^{-1}$ . The wind became SE and stronger on 6 April from 10:00 to 22:00 ( $9 \text{ m s}^{-1}$ ), then mainly N and weaker from 7 to 9 April ( $4 \text{ m s}^{-1}$ ). During the third field campaign, there was a NNW wind from 8:00 on 27 April to 10:00 on 28 April, then mainly a S wind until 29 April (overall speed ca.  $3 \text{ m s}^{-1}$ ). During the summer campaign, a very strong NW wind event started on 23 July and persisted until 27 July, with an overall speed of  $8 \text{ m s}^{-1}$ . The wind became SW on 28 July ( $6 \text{ m s}^{-1}$ ) and then reverted to NW ( $5 \text{ m s}^{-1}$ ). On 2–3 November there was a NW wind of overall  $6.5 \text{ m s}^{-1}$  and

then, on 4–5 November during the late autumn cruise, a variable wind with dominant N and NE directions and an overall speed of  $2 \text{ m s}^{-1}$ .

### Vertical salinity profiles

For the vertical salinity profiles recorded in the vicinity of the Mesurho buoy (Fig. 3), the sampling stations had a bottom depth varying from 20 to 25 m and, therefore, the water depth was normalized to (i.e. divided by) the bottom depth. Salinity varied strongly in the upper half of the water column (0 to  $-0.5$  normalized depth in Fig. 3), and was consistently high in the lower half. The depth at which the salinity was lower than 37 PSU is considered to demarcate the depth of the river plume (i.e. less saline waters). On this basis, the salinity profiles show that plume thickness is season-dependent. Consistent with the freshwater discharge varying substantially from  $850 \text{ m}^3 \text{ s}^{-1}$  in late July to more than  $2,800 \text{ m}^3 \text{ s}^{-1}$  in early April 2010 (Fig. 2), the river plume was almost 8 m thick on 9 April and 6 m thick on 28 April. Intermediate values were observed on 17 March and 29 July—less than 4 m in each case. Plume thickness was even less than 3 m on 4 November.

The strongest salinity gradient was observed within the upper 1 m of the water column (0.3–1 m depth); it was 4 to 5 times weaker between 1 and 2 m depth. Below 2 m depth, water salinity was almost constant and typical of the surrounding coastal waters, i.e. generally higher than 36 PSU irrespective of river discharge conditions, except during the

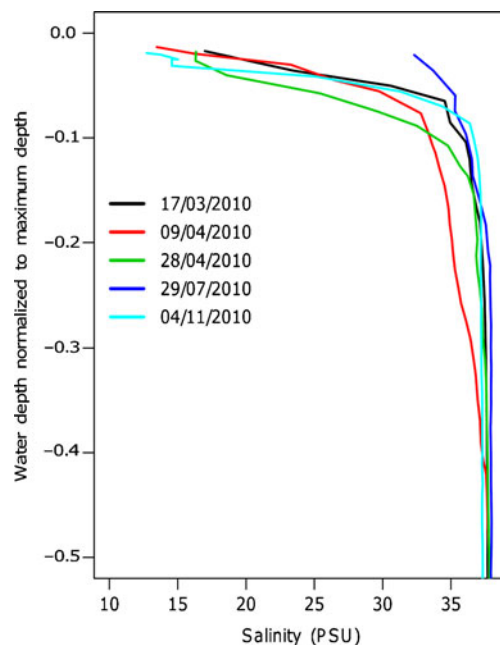


**Fig. 3** Vertical salinity profiles in the vicinity of the Mesurho buoy near the Rhône River mouth during the five campaigns of 2010 (bottom depths varied between 20 and 25 m; to facilitate comparison, water depth has been normalized to bottom depth in each case)

spring flood event of 9 April. Minimum values of surface salinity were observed on 9 April and 4 November (less than 14 and 13 PSU respectively), immediately after two peak flood events. The highest surface salinity was recorded on 29 July (32 PSU), associated with low river freshwater discharge in summer. Measurements of salinity carried out on 17 March and 28 April were typical of springtime situations, associated with intermediate discharge. Note that two peaks of freshwater discharge higher than  $3,000 \text{ m}^3 \text{ s}^{-1}$  occurred 10 and 20 days earlier respectively.

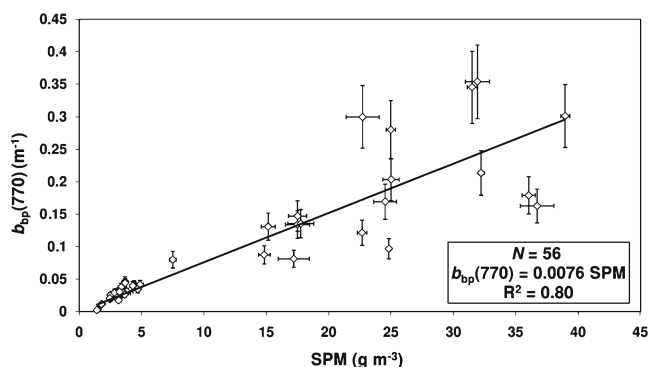
#### Light backscattering by particles versus SPM concentration

Figure 4 shows the linear regression obtained between the  $b_{\text{bp}}(770)$  coefficient (in  $\text{m}^{-1}$ ) and SPM concentration (in  $\text{g m}^{-3}$ ), both averaged within the upper 1 m of the water column. Although this complete dataset covers various seasonal conditions, it is well represented by a single linear regression ( $R^2=0.80$ ,  $N=56$ ):

$$b_{\text{bp}}(770) = 0.0076 \times \text{SPM} \quad (3)$$

Table 1 summarizes the linear regressions established for each campaign of 2010, based on their slopes  $b_{\text{bp}}(770)/\text{SPM}$  ( $\text{m}^2 \text{ g}^{-1}$ ). Note that summer data are not available due to a malfunctioning of the CTD sensor during that campaign. The maximum regression slope of  $0.0089 \text{ m}^2 \text{ g}^{-1}$  observed during early spring moderate outflow differs only slightly (15%) from the minimum value of  $0.0075 \text{ m}^2 \text{ g}^{-1}$  observed during the spring flood event.

Mean POC/SPM ratios (Table 1) were lowest during the November 2010 campaign (autumn flood event, 2.4%) and highest on 28–29 April (mid-spring intermediate outflow, 11%). Intermediate values of 5.4 and 3.2% occurred on 16–17 March (early spring intermediate outflow) and 9 April (spring flood event) respectively. Mean chl *a* concentrations (Table 1) did not vary markedly during the three spring cruises spanning March–April of 2010, ranging between  $0.81 \text{ mg m}^{-3}$  on 28–29 April and  $1.06 \text{ mg m}^{-3}$  on 9 April.



**Fig. 4** Scatterplot of  $b_{\text{bp}}(770)$  versus SPM concentration. The linear regression has zero intercept. Error bars Standard deviations

During the flood events, the  $b_{\text{bp}}$  sensor mounted on the CTD rosette saturated at 532 nm for SPM concentrations greater than  $15 \text{ g m}^{-3}$ . For SPM concentrations lower than this threshold, the following linear regression ( $R^2=0.80$ ,  $N=38$ ) was obtained between  $b_{\text{bp}}(532)$  and SPM (both averaged for the upper 1 m of the water column):

$$b_{\text{bp}}(532) = 0.0119 \times \text{SPM} \quad (4)$$

Because of this saturation problem at 532 nm, the  $b_{\text{bp}}$  signal recorded in the near-infrared band, namely 770 nm, was used to estimate SPM concentrations. Another reason for selecting 770 nm is that the inversion of the  $R_{\text{rs}}$  signal into  $b_{\text{bp}}$  is easier in the near-infrared spectral region, where only light absorption by pure seawater and light backscattering by particles are significant (Babin and Stramski 2002).

#### Mean $b_{\text{bp}}(770)$ near the surface and at depth

In order to determine whether ocean colour satellite observations limited to 1 m below the water surface can serve to predict SPM concentrations deeper in the river plume, the relationship between  $b_{\text{bp}}(770)$  averaged over 0.3–1.0 m depth (hereafter referred to as  $\langle b_{\text{bp}}(\text{surf}) \rangle$ ) and  $b_{\text{bp}}(770)$  averaged over the entire vertical layer of the plume (hereafter referred to as  $\langle b_{\text{bp}}(\text{plume}) \rangle$ ) was examined. Here again, the river plume depth was defined as that of salinity  $<37$  PSU (cf. above).

The results revealed that mean river plume depth varied markedly during the four spring and autumn campaigns (Table 2). Maximum plume depth was during the spring flood event (6 m) and minimum depth during the autumn flood event (1.8 m). Intermediate values were observed at moderate freshwater discharge, varying between 3.5 and 5 m. Calculating the ratio  $\langle b_{\text{bp}}(\text{plume}) \rangle / \langle b_{\text{bp}}(\text{surf}) \rangle$  indicated that, for higher plume depth values (5–6 m),  $\langle b_{\text{bp}}(\text{plume}) \rangle$  was almost half of  $\langle b_{\text{bp}}(\text{surf}) \rangle$  (Table 2). For lower plume depth values (1.8–3.5 m),  $\langle b_{\text{bp}}(\text{plume}) \rangle$  was only 5–15% smaller than  $\langle b_{\text{bp}}(\text{surf}) \rangle$ .

#### Vertical $b_{\text{bp}}(770)$ and $b_{\text{bp}}(532)$ profiles

Vertical variations in  $b_{\text{bp}}(770)$  were examined based on profiles recorded from aboard the ship near the Mesurho buoy at variable time intervals throughout the day during the field campaigns, selected examples being reported in Fig. 5. Irrespective of freshwater discharge conditions (cf. Fig. 2),  $b_{\text{bp}}(770)$  values were high at the surface and decreased continuously within the upper 5 m of the water column.

Vertical  $b_{\text{bp}}(770)$  profiles repeated at time intervals varying from several minutes to 24 h exhibit overall similar patterns within the upper 5 m and also at greater depths

**Table 1** Minimum and maximum SPM concentrations (dry mass basis), slopes and coefficients of determination ( $R^2$ ) of linear regressions between  $b_{bp}(770)$  and SPM, mean chl a concentrations (dry massbasis), and mean POC/SPM ratios in surface waters (upper 1 m) for four field campaigns (*NA* not available)

Field campaign (2010)	<i>N</i>	SPM min.–max. ( $\text{g m}^{-3}$ )	$b_{bp}(770)/\text{SPM}$ ( $\text{m}^2 \text{g}^{-1}$ )	$R^2$	Mean chl a ( $\text{mg m}^{-3}$ )	Mean POC/SPM (%)
16–17 March	18	2.47–4.86	0.0089	0.62	1.03±0.16	5.4±1.0
9 April	8	11.78–25.00	0.0075	0.94	1.06±0.16	3.2±0.4
28–29 April	14	1.40–3.63	0.0085	0.74	0.81±0.35	11.0±3.6
4–5 November	16	3.15–38.96	0.0076	0.51	NA	2.4±1.2

(see examples of late morning and early afternoon profiles in Fig. 5a–c, e). From 5 m to at least 18 m depths, the  $b_{bp}(770)$  values remained relatively low under all discharge conditions.

The occasional occurrence of a high-turbidity bottom nepheloid layer (BNL) can be inferred in terms of a sharp increase in the  $b_{bp}(770)$  signal. This was particularly noticeable in summer 2010 when the freshwater discharge was at its lowest: near the bottom (25 m depth), the  $b_{bp}(770)$  value was almost 2 times higher than that observed near the surface (0.04 and  $0.025 \text{ m}^{-1}$  respectively; Fig. 5d). At times of moderate discharge in spring 2010, in contrast, the bottom  $b_{bp}(770)$  values were approx. half those recorded near the surface (Fig. 5a, profile labelled 14:56 and Fig. 5c, profile labelled +24 h). During the spring and autumn flood events, the bottom  $b_{bp}(770)$  signals were as much as 5–6 times lower than the surface values (Fig. 5b and e, profile labelled 15:20).

The surface (surf) versus bottom (btm)  $b_{bp}(770)$  ratio of 0.5 recorded at minimum river freshwater discharge ( $<1,000 \text{ m}^3 \text{ s}^{-1}$ ) indicates that a high proportion of the total suspended load was confined to the BNL at the time and, thus, would not have been detected by ocean colour satellite observations. At intermediate discharge (ca.  $1,500 \text{ m}^3 \text{ s}^{-1}$ ), a ratio of about 2 indicates that one third of the total SPM load would have remained undetected. During flood events (discharge  $>2,000 \text{ m}^3 \text{ s}^{-1}$ ),  $b_{bp}(\text{surf})/b_{bp}(\text{btm})$  ratios of about 5–6 imply that the limitation of satellite data to surface waters would be of less importance in terms of water column extrapolation in such cases.

The data recorded by the ProvBio in the period 15 April to 24 June 2010 (cf. Fig. 2) are reported in Fig. 6. Note that the float was sometimes positioned as far as 20 km from the Mesurho buoy, whereas the research vessel remained within ca. 5 km of the buoy. The dataset comprises  $b_{bp}(532)$

profiles measured every 6 h between sunrise and sunset over 48 h at essentially the same location on 15–16 April, 7–8 May, 12–13 May and 23–24 June 2010. During each 2-day period, the six vertical profiles were very similar. Some extraneous data points are considered to be artefacts. The profiles can be subdivided into three sectors: a surface layer with high  $b_{bp}(532)$  values, an intermediate layer with lower values, and a BNL where  $b_{bp}(532)$  values are again high.

#### Seasonal $b_{bp}(770)$ and $b_{bp}(532)$ vertical profiles

Under moderate springtime freshwater discharge conditions (Fig. 5a, c), a maximum  $b_{bp}(770)$  value of about  $0.04 \text{ m}^{-1}$  was recorded at the surface. During the autumn peak flood, the corresponding value was almost 10 times as high (Fig. 5e), with  $b_{bp}(770)$  values decreasing by a factor of 2 between 0.3 and 1 m depth. This was to be expected, seeing that the short autumnal flood resulted in a sharp increase in river outflow from 1,000 to more than  $3,300 \text{ m}^3 \text{ s}^{-1}$  over 2 days, followed by an abrupt decrease (Fig. 2). Note that, spanning the spring and autumnal flood events, freshwater discharge continuously exceeded  $2,000 \text{ m}^3 \text{ s}^{-1}$  for 15 and 3 days respectively, with a peak of about  $3,300 \text{ m}^3 \text{ s}^{-1}$  in both cases.

During the spring flood event, the vertical  $b_{bp}(770)$  gradient was  $0.047 \text{ m}^{-2}$  within the upper 5 m. In contrast, the autumnal flood event induced a very thin stratified layer with a stronger gradient of  $0.236 \text{ m}^{-2}$  between 0.3 and 1 m depth, and only  $0.015 \text{ m}^{-2}$  between 1 and 5 m depth. It is important to note that the  $b_{bp}(770)$  values at 1 m depth were similar in both cases.

In summer (Fig. 5d), freshwater discharge was among the lowest for the year 2010:  $850 \text{ m}^3 \text{ s}^{-1}$  (Fig. 2). The values were actually less than  $1,500 \text{ m}^3 \text{ s}^{-1}$  during the 33 days

**Table 2** Mean Rhône River plume depths, and ratios between  $b_{bp}(770)$  values averaged over the whole thickness of the river plume ( $\langle b_{bp}(\text{plume}) \rangle$ ) and over 0.3–1 m depth ( $\langle b_{bp}(\text{surf}) \rangle$ ). *N* Number of profiles

Field campaign (2010)	Mean river plume depth, <i>z</i> (m)	$\langle b_{bp}(\text{plume}) \rangle / \langle b_{bp}(\text{surf}) \rangle$
16–17 March, <i>N</i> =30 (intermediate outflow)	3.5±0.7	0.855±0.079
9 April, <i>N</i> =12 (spring flood event)	6.0±1.0	0.612±0.230
28–29 April, <i>N</i> =16 (intermediate outflow)	5.0±1.5	0.527±0.152
4–5 November, <i>N</i> =17 (autumn flood event)	1.8±0.6	0.946±0.060

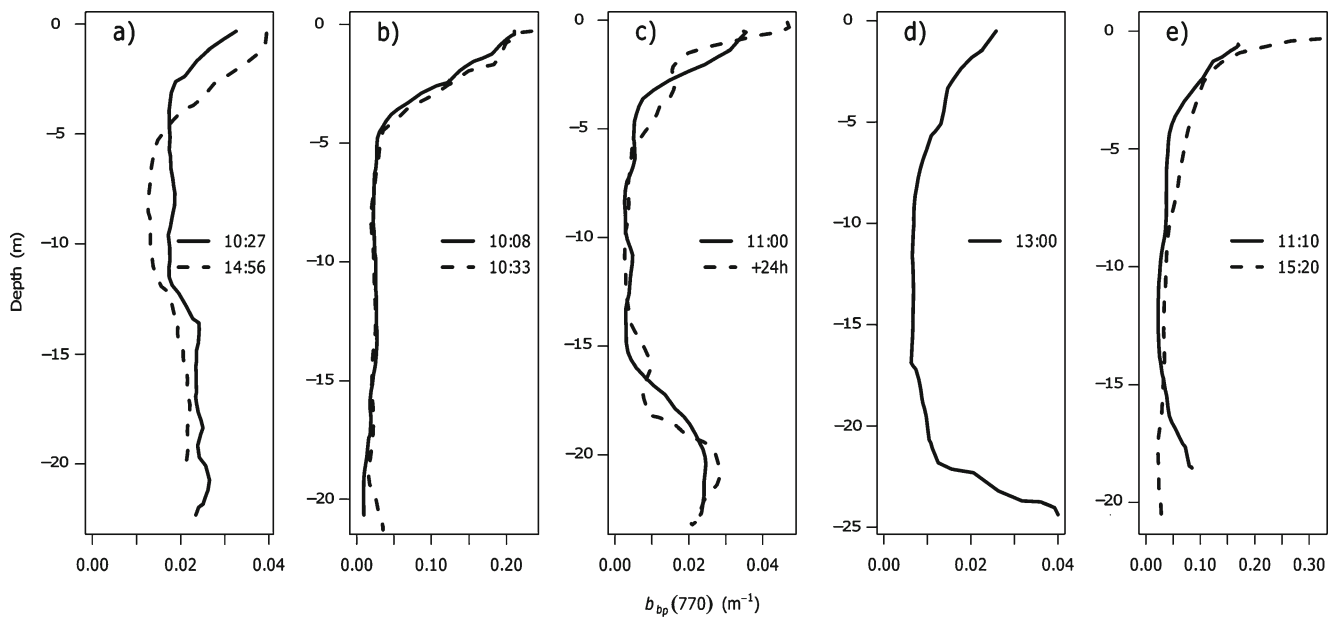


**Fig. 5** Variations in  $b_{bp}(770)$  as a function of water depth in the late morning and early afternoon of **a** 17 March, **b** 9 April, **c** 28 April, **d** 29 July and **e** 4 November 2010

preceding the field campaign.  $b_{bp}(770)$  values were highest at the surface and slightly decreased down to 10 m depth.

For the 8 days of study, the vertical  $b_{bp}(532)$  profiles recorded by the ProvBio float (Fig. 6) revealed surface values which were low on 15–16 April ( $<0.01 \text{ m}^{-1}$ ) relative to 12 May (maximum  $0.07 \text{ m}^{-1}$ ) when a flood event occurred (Fig. 2). A flood reaching values of  $3,000 \text{ m}^3 \text{ s}^{-1}$  occurred on 18 June. On 23–24 June, the  $b_{bp}(532)$  signal was highest within surface waters and decreased down to 20 m depth, associated with a very strong NW wind ( $10 \text{ m s}^{-1}$ ) which evidently mixed the surface layer. On 15–16 April during calm wind conditions, in contrast,  $b_{bp}(532)$  values decreased more strongly with depth (i.e. minimum slightly deeper than 10 m).

#### Large-scale horizontal $b_{bp}(770)$ and $b_{bp}(532)$ trends

Figure 7 shows the horizontal variations in  $b_{bp}(770)$  recorded within the surface plume and the BNL under variable seasonal conditions as the ship drifted freely from the river mouth to 7 km offshore.  $b_{bp}(770)$  values at 1 m depth decreased from 0.028 to  $0.020 \text{ m}^{-1}$  offshore along the transect on 17 March, and from 0.270 to  $0.106 \text{ m}^{-1}$  on 9 April (Fig. 7b, c), corresponding to horizontal  $b_{bp}(770)$  gradients of  $0.0022$  and  $0.0447 \text{ m}^{-1} \text{ km}^{-1}$  respectively, i.e. offshore decreases of 8 and 17% per kilometre during these moderate and peak flood events respectively. Note that in both cases the gradient was calculated along a distance of 3 km for a similar ship trajectory. Maximum SPM concentrations were less than 5 and  $25 \text{ g m}^{-3}$  during the moderate and peak flood events respectively (Table 1).

On both 17 March and 9 April (i.e. before and during a spring flood event, Fig. 2), the ship drifted southwards and slightly westwards (Fig. 7a, b). Wind conditions were also similar, with a N wind in the morning rotating to S from about noon onwards. On these 2 days, the river plume was constrained within the upper 5 and 6 m of the water column.

On 17 March, 9 April and 28 July (Fig. 7a, b, d), high  $b_{bp}(770)$  values observed close to the bottom revealed the occurrence of a BNL,  $b_{bp}(770)$  reaching  $0.05 \text{ m}^{-1}$  within this  $<10 \text{ m}$  thick bottom layer. There was a distinct southeast drift direction on 28 July (Fig. 7d), following a strong NW wind event during the 5 days preceding the campaign combined with a W wind during the campaign. During the autumnal flood event of 4 November (Fig. 7e), the horizontal  $b_{bp}$  gradient was  $0.0264 \text{ m}^{-1} \text{ km}^{-1}$ . It should be noted that the horizontal  $b_{bp}(770)$  gradients observed during the spring and autumn flood events cannot be rigorously compared because the ship drift trajectories and, thus, the water masses exported by the river plume were not identical.

## Discussion and conclusions

### Light backscattering by particles as SPM proxy

Despite the marked temporal variations in surface SPM composition revealed in terms of POC/SPM ratios, the strong relationship between surface  $b_{bp}(770)$  and SPM concentration observed for the pooled dataset (Eq. 3) suggests that, if any, POC content has only a weak impact on the SPM backscattering efficiency in the study area. Evidently,

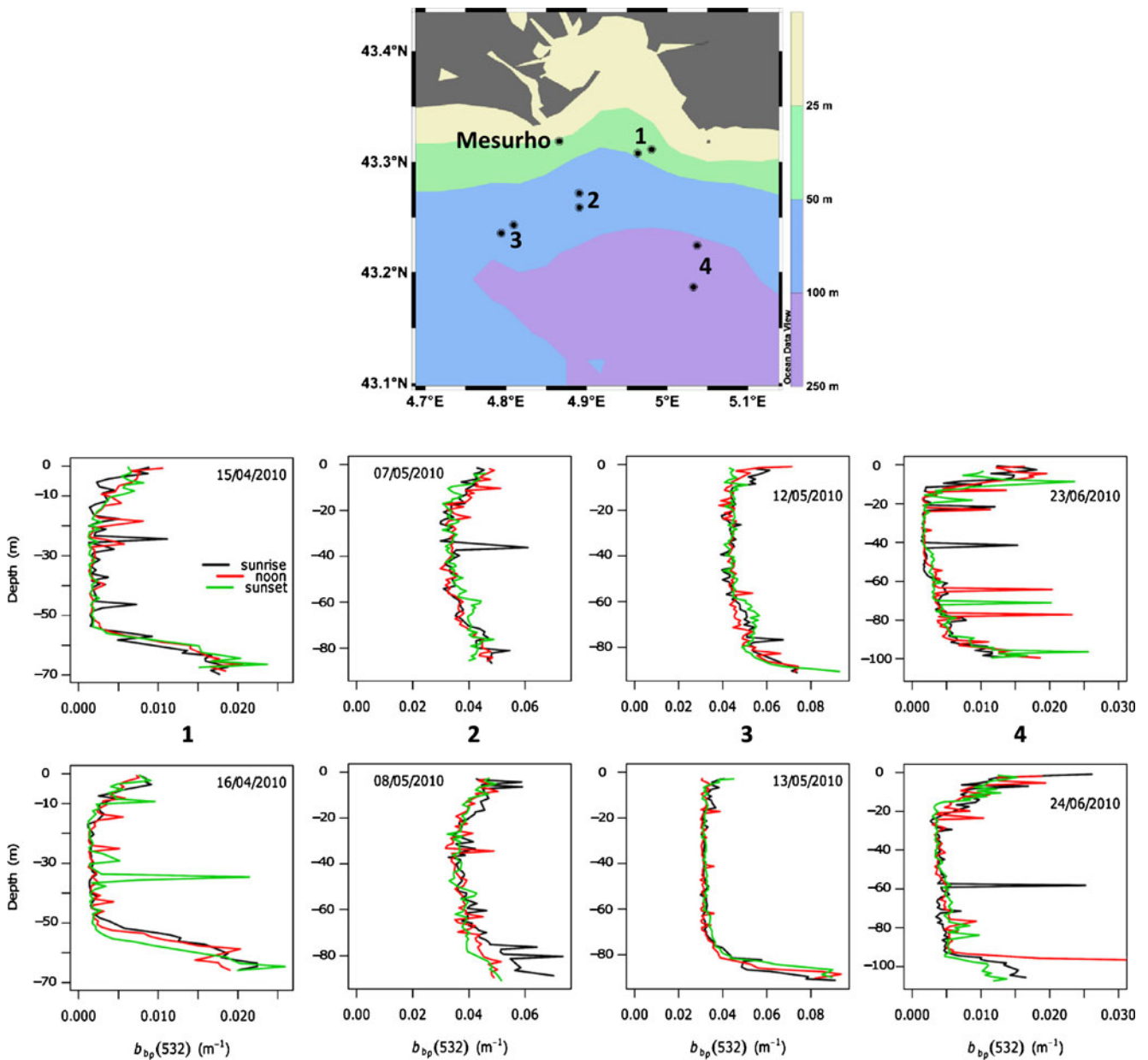


**Fig. 6** Variations in  $b_{bp}(532)$  as a function of water depth over four 2-day measuring periods in April, May and June 2010, recorded by means of ECO BB sensors mounted on an autonomous profiling float

Eq. 3 can serve to predict surface SPM concentrations based on  $b_{bp}$  irrespective of Rhône River freshwater discharge levels.

The finding that surface mean chlorophyll a concentrations were fairly similar despite fluctuations in river discharge during the three spring campaigns suggests that riverine nutrient inputs are not sufficiently high to measurably promote phytoplankton growth in the river plume. This is supported by data from Naudin et al. (2001), who reported lower nutrient concentrations for the Rhône River plume as compared to other European river plumes and estuaries. Another explanation (cf. Naudin et al. 2001) is that many

which drifted between 7 and 20 km offshore the river mouth. Three profiles were recorded daily at 08:00, 12:00 and 18:00 hours (local time)

phytoplankton species grow better slightly deeper in the water column where salinity is higher. The implication for the  $b_{bp}$  vs. SPM relationship is that it is not straightforward to extract information on chl a concentration from the backscattering coefficient of the Rhône River plume.

Equations 3 and 4 convincingly demonstrate that robust relationships can be obtained between SPM concentration and the particulate backscattering coefficient both in the visible and near-infrared spectral bands. Irrespective of wavelength, the  $b_{bp}$  coefficient depends on particle concentration, composition (refractive index) and size distribution (Neukermans et al. 2012). Organic-rich (phytoplankton) and

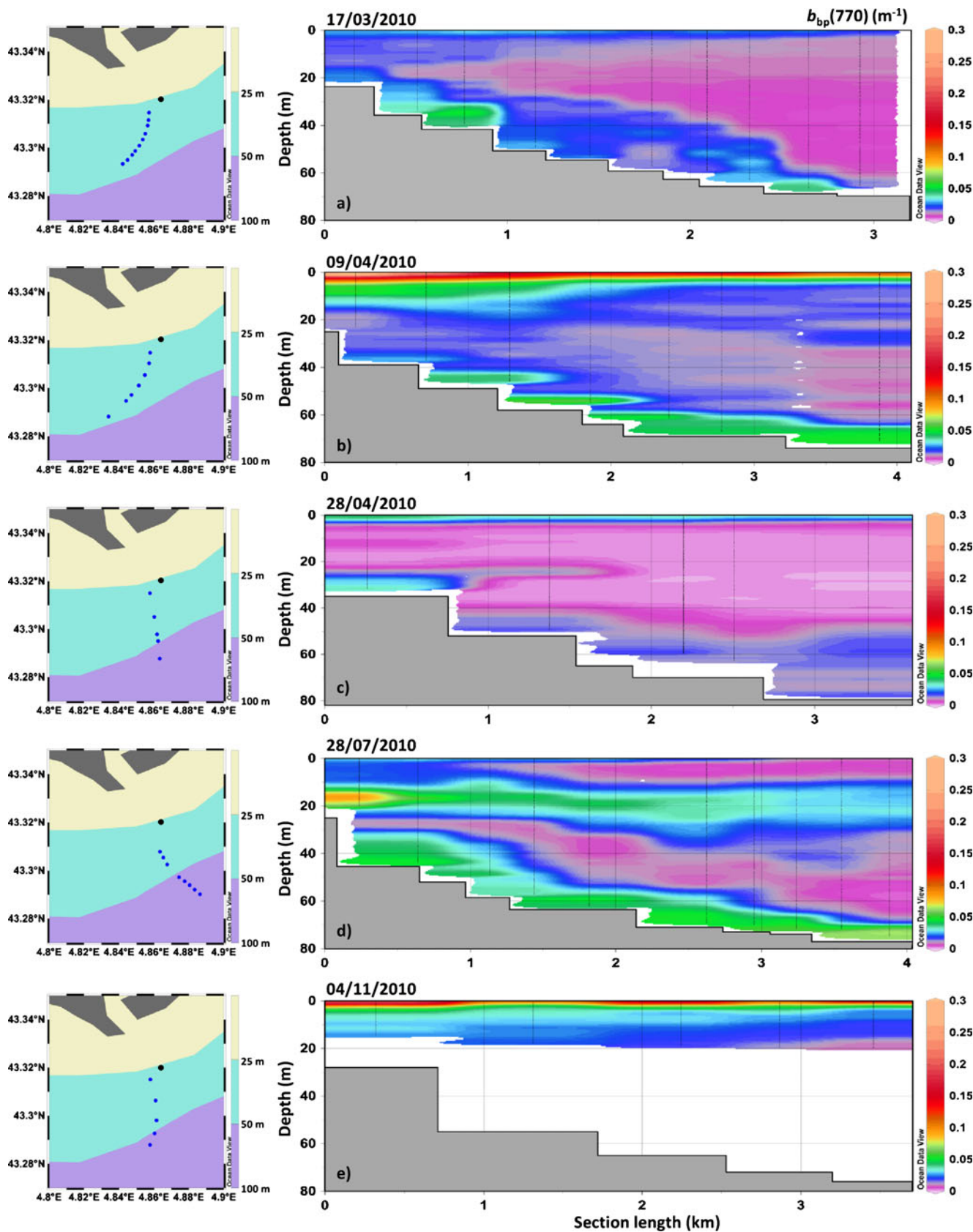


**Fig. 7** Variations in  $b_{bp}(770)$  as a function of water depth at various distances from the Mesurho buoy (black dot) near the river mouth. Measurements were from aboard ship freely drifting over distances of

3–4 km on **a** 17 March, **b** 9 April, **c** 28 April, **d** 28 July and **e** 4 November 2010 (R. Schlitzer, Ocean Data View, <http://odv.awi.de>, version 4.3.5)

mineral-rich (sediments) suspended particles are usually mixed within surface coastal waters, with respective contributions on light backscattering which vary depending on river inputs, resuspension processes and bloom events. However, fine mineral particles are known to be the most efficient in terms of light backscattering because of their high refractive index (Stramski et al. 2001), which explains why an overall robust relationship was obtained for the Rhône River plume. Thus, the results show that light backscattering by particles can be used as a convenient proxy to estimate SPM concentration at the river mouth and within the plume, with direct implications for ocean colour remote sensing. It appears to be much more difficult to extract relevant information on particle composition. Satellite and Mesurho buoy data represent complementary tools yielding synoptic views of Rhône River plume spatial dimensions and SPM concentrations.

#### Retrieval of plume $b_{bp}(770)$ from near-surface data

The results indicate that deriving plume  $b_{bp}(770)$  from  $b_{bp}(770)$  averaged over the upper 1 m is possible but depends on plume thickness. This is straightforward when plume thickness is relatively small (i.e. <3.5 m) and more problematic otherwise (thickness of 5–6 m). Similar to the Rhône River in terms of SPM concentrations, Ouilon (2003) showed that solar light penetration within the Ebro River plume (Spain) is highly wavelength-dependent: typically, the longer the wavelength, the thinner the surface layer which can be viewed by a satellite sensor.

For the Rhône River, the present results provide evidence that plume depth is not necessarily related to the magnitude of discharge but rather to the duration of a flood event. During a short flood event, plume depth is less pronounced. On this basis, particular attention should be paid to a priori knowledge of measured river freshwater discharge in the study area during the course of the year, to determine whether satellite data can be used to estimate SPM concentrations at depth in the river plume.

#### Vertical SPM trends

The present results demonstrate that, depending on river discharge, satellite-derived SPM concentrations in surface waters are usually not representative of water column particle loads (cf. Fig. 5). Aloisi et al. (1979, 1982) showed that solid matter in GoL coastal waters is constrained mainly to the BNL, its dynamics being linked to the general circulation pattern in the gulf. However, the present study found that most of the SPM load is confined within surface waters close to the river mouth during flood events. Seeing that Antonelli et al. (2008) have demonstrated that flood events are responsible for 80% of total Rhône River particulate

inputs in the GoL, these findings imply that satellite remote sensing data can be efficiently exploited to estimate most of the annual riverine SPM flux into the gulf.

Under non-flood, windless conditions, vertical SPM concentration profiles provide evidence of change from a well-defined two-layer stratification pattern to a complex multi-layered pattern. In such cases, measurements confined to the upper 1 m cannot be extrapolated to deeper in the water column. Moreover, there were only slight hourly/daily variations in vertical SPM profiles under non-flood and, for that matter, also flood conditions (Figs. 5 and 6). Therefore, ocean colour remote sensing snapshots acquired typically towards noon on windless days are appropriate to map large-scale daily surface SPM trends. This is facilitated by tidal forcing being weak in the GoL, contrasting with, for example, estuaries such as the Gironde (France) where daily and fortnightly tidal cycles are associated with rapid mixing and strong short-term variations in surface SPM concentrations (e.g. Doxaran et al. 2009).

Rough weather commonly promotes particle mixing, vertical deepening, and a horizontal expansion of the Rhône River plume (Naudin et al. 2001; Ulses et al. 2008). This has been confirmed in the present study based on data from the autonomous ProvBio float, complementing information gathered from aboard ship under calmer weather conditions. Offshore ProvBio profiles showed maximum  $b_{bp}$  values extending from the surface down to 10–20 m depth, which is 2–4 times deeper than for shipboard profiles run near the coast: the further the distance from the coast, the thicker the surface layer impacted by riverine particle export. The BNL layer is also thicker offshore—20 m, compared to the 10 m recorded from the ship close to the river mouth. Maximum ProvBio  $b_{bp}$  values were similar for the BNL and surface waters, confirming the important SPM transport occurring near the seabed.

#### Seasonal trends in vertical SPM patterns

Irrespective of seasonal variations in Rhône River freshwater discharge, the  $b_{bp}(770)$  signal was systematically higher within surface waters, decreasing with depth. In contrast, other characteristics of the  $b_{bp}$  signal varied strongly during the 2010 study period, plausibly explained by variable freshwater discharge in combination with flood duration and wind conditions.

During a long flood event (15 days of discharge  $>2,000 \text{ m}^3 \text{ s}^{-1}$ ), the vertical  $b_{bp}(770)$  gradient remained stable at 0.3–5 m depth, which was not the case during a short flood event (3 days of discharge  $>2,000 \text{ m}^3 \text{ s}^{-1}$ ). Compared to a long flood event, the gradients were 5 times stronger at 0.3–1 m depth, and 3 times weaker at 1–5 m depth. Evidently, freshwater discharge impacts the magnitude of  $b_{bp}(770)$  values, whereas the duration of flood

events has a strong influence on the plume vertical thickness and SPM distribution within the subsurface layer. Brief, intense flood events would enhance bottom erosion and SPM transport, and be associated with relatively thin river plumes (upper few metres). Data for the upper 1 m could then justifiably serve to predict SPM concentrations deeper in the water column. This would apply episodically also to the summer situation, characterized by lowest surface  $b_{bp}(770)$  values and when wind events would be the dominant physical factor enhancing SPM mixing. Within this context, the 2010 summer is representative of the last decades in terms of river freshwater discharge.

#### SPM dynamics in the plume and nepheloid layers

Seeing that  $b_{bp}$  is a good proxy of SPM concentration in the Rhône River plume (see Eq. 3), horizontal  $b_{bp}$  gradients reflect the spatial heterogeneity in SPM concentration from the Rhône River mouth to several kilometres offshore, and this can be interpreted in terms of freshwater discharge and wind conditions. The horizontal  $b_{bp}(770)$  gradients identified in the present study suggest that particles exported during peak flood events settle rapidly close to the coast, which is not the case for moderate flood events. This could be explained by the former being associated with overall larger particles. Measurements of particle size distributions would be helpful to verify this aspect.

To date, transport of particles within the BNL has been poorly documented in the vicinity of the Rhône River mouth. This is due to the stratified nature of the flow near the seabed and to technical difficulties (e.g. Aloisi et al. 1979; Naudin and Cauwet 1997). Thus, precise estimates of BNL thickness are often not possible from aboard ship because the distance between the deepest in situ measurements and the seabed cannot always be assessed accurately enough. The ProvBio sensor does not have this drawback because, if wished, it can ground essentially at the seabed. In the present study, this was the case at night (cf. Materials and methods section). The results reveal that, under low river outflow conditions and particularly with weak winds, most of the SPM offshore transport takes place within the BNL, rather than in the surface layer (Fig. 7).

Ocean colour MERIS satellite data available for the time-frame of the 2010 field campaigns provide complementary evidence of large-scale plume spatial characteristics plausibly explained by, amongst others, the wind pattern (Fig. 1). For example, the two flood events are associated with different plume orientations consistent with the NW wind of 5 April pushing the river plume offshore, the reverse being the case on 5 November (Fig. 1c, f). The plume had rather similar SPM concentration gradients in the close vicinity of the mouth but not further offshore. Under moderate and low discharge conditions (Fig. 1b, d, e), satellite-based

surface SPM concentrations at the river mouth were about one order of magnitude lower than those observed during flood conditions. On 14 March, the plume was pushed southwards by a strong NNW wind (the mistral,  $6 \text{ m s}^{-1}$ ) and, on 28 July, a NW wind led to a plume oriented SE. Such wind-induced satellite-based patterns are consistent with the findings of Naudin et al. (1997, 2001) who reported that the buoyancy of the Rhône River plume favours a quasi-instantaneous response to wind. Qualitatively, the horizontal SPM concentration gradients retrieved from remote sensing and in situ measurements were similar.

In conclusion, the findings of the present study make a solid contribution to ongoing efforts to improve an existing hydrodynamic model by incorporating high-resolution temporal variations in three-dimensional SPM fluxes based on data from remote sensing, in situ ship and profiling float measurements, and the fixed Mesurho buoy at the Rhône River mouth. The findings should prove useful in adapting this approach to similar settings.

**Acknowledgements** We are very grateful to I. Pairaud and R. Verney (IFREMER), as well as the crew of the RV Antédon II for their support and help during the field campaigns. We would like to thank two reviewers for helpful comments which contributed to improve the paper. This study was funded by the Centre National d'Etudes Spatiales (CNES) through the Provpanache project, by the Programme National de Télédétection Spatiale (INSU-CNRS) and by the Groupe Mission MERCATOR/CORIOLIS. We are also grateful to the Université Pierre et Marie Curie for funding the PhD grant of T. Lorthiois.

#### References

- Acker JG, Harding LW, Leptoukh G, Zhu T, Shen S (2005) Remotely-sensed chl a at the Chesapeake Bay mouth is correlated with annual freshwater flow to Chesapeake Bay. *Geophys Res Lett* 32:L05601. doi:10.1029/2004GL021852
- Aloisi JC, Millot C, Monaco A, Pauc H (1979) Dynamique des suspensions et mécanismes sédimentogénétiques sur le plateau continental du Golfe du Lion. *C R Acad Sci Paris II* 289:879–882
- Aloisi JC, Cambon JP, Carbonne J, Cauwet G, Millot C, Monaco A, Pauc H (1982) Origine et rôle du néphéloïde profond dans le transfert des particules en milieu marin. Application au Golfe du Lion. *Oceanol Acta* 5:481–491
- Antonelli C, Eyrolle F, Rolland B, Provansal M, Sabatier F (2008) Suspended sediment and  $^{137}\text{Cs}$  fluxes during the exceptional December 2003 flood in the Rhone River, southeast France. *Geomorphology* 95(3/4):350–360
- Babin M, Stramski D (2002) Light absorption by aquatic particles in the near-infrared spectral region. *Limnol Oceanogr* 47(3):911–915
- Boss E, Pegau WS (2001) Relationship of light scattering at an angle in the backward direction to the backscattering coefficient. *Appl Optics* 40(30):5503–5507
- Bourrin F, Durrieu de Madron X (2006) Contribution to the study of coastal rivers and associated prodeltas to sediment supply in the Gulf of Lions (NW Mediterranean Sea). *Life Environ* 56(4):307–314

- Broche P, Devenon JL, Forget P, Maistre JC, Naudin J-J, Cauwet G (1998) Experimental study of the Rhone plume. Part I: physics and dynamics. *Oceanol Acta* 21:725–737
- Chami M, Marken E, Stamnes JJ, Khomenko G, Korotaev G (2006) Variability of the relationship between the particulate backscattering coefficient and the volume scattering function measured at fixed angles. *J Geophys Res* 111:C05013. doi:10.1029/2005JC003230
- Demarcq H, Wald L (1984) La dynamique superficielle du panache du Rhône d'après l'imagerie infrarouge satellitaire. *Oceanol Acta* 7(2):159–162
- Doerffer R, Schiller H (2007) The MERIS Case 2 water algorithm. *Int J Remote Sensing* 28(3/4):517–535
- Doxaran D, Froidefond JM, Castaing P, Babin M (2009) Dynamics of the turbidity maximum zone in a macrotidal estuary (the Gironde, France): observations from field and MODIS satellite data. *Estuarine Coastal Shelf Sci* 81:321–332
- Doxaran D, Claustre H, Babin M, Lorthiois T, Poteau A (2011) Use of ProvBio floats to study the dynamics of suspended particles in river plumes: the Provpanache project. *Coriolis Newslett* 7(41):13–17
- Dufois F (2008) Modélisation du transport particulaire dans le Golfe du Lion en vue d'une application au devenir des traceurs radioactifs issus du Rhône. Thèse de Doctorat, Université du Sud Toulon Var
- Durrieu de Madron X, Abassi A, Heussner S, Monaco A, Aloisi JC, Radakovitch O, Giresse P, Buscaill R, Kerherve P (2000) Particulate matter and organic carbon budgets for the Gulf of Lion (NW Mediterranean). *Oceanol Acta* 23(6):717–730
- Dyer KR (1986) Coastal and estuarine sediment dynamics. Wiley, Chichester
- Eisma D, Bernhard P, Cadée GC, Ittekkot V, Kalf J, Laane R, Martin JM, Mook WG, Van Put A, Schuhmacher T (1991) Suspended matter particle size in some West-European estuaries; part II: a review on floc formation and break up. *Neth J Sea Res* 28(3):215–220
- Estournel C, Broche P, Marsaleix P, Devenon J, Auclair F, Vehil R (2001) The Rhone River plume in unsteady conditions: numerical and experiment results. *Estuarine Coastal Shelf Sci* 53(1):25–38
- Estournel C, Durrieu de Madron X, Marsaleix P, Auclair F, Julliaud C, Vehil R (2003) Observation and modeling of the winter coastal oceanic circulation in the Gulf of Lion under wind conditions influenced by the continental orography (FETCH experiment). *J Geophys Res* 108:8059. doi:10.1029/2001JC000825
- Forget P, Ouillon S (1998) Surface suspended matter off the Rhône river mouth from visible satellite imagery. *Oceanol Acta* 21(6):739–749
- Forget P, Ouillon S, Lahet F, Broche P (1999) Inversion of reflectance spectra of non-chlorophyllous turbid coastal waters. *Remote Sensing Environ* 68:264–272
- Forget P, Broche P, Naudin JJ (2001) Reflectance sensitivity to solid suspended sediment stratification in coastal water and inversion; a case study. *Remote Sensing Environ* 77:92–103
- Gordon HR, Brown OB, Jacobs MM (1975) Computed relation between the inherent and apparent optical properties of a flat homogeneous ocean. *Appl Optics* 14:417–427
- Lamy A, Millot C, Molines JM (1981) Bottom pressure and sea level measurements in the Gulf of Lions. *J Phys Oceanogr* 11:394–410
- Le Reste S, André X, Claustre H, D'Ortenzio F, Poteau A (2009) First success of ProvBio floats. *Coriolis Newslett* 5:5–8
- Maritorena S, Siegel DA, Peterson AR (2002) Optimization of a semi-analytical ocean color model for global-scale applications. *Appl Optics* 41(15):2705–2714
- Milliman JD, Farnsworth KL (2011) River discharge to the coastal ocean: a global synthesis. Cambridge University Press, Cambridge
- Millot C (1990) The Gulf of Lions' hydrodynamics. *Cont Shelf Res* 10(9/11):885–894
- Naudin JJ, Cauwet G (1997) Transfer mechanisms and biogeochemical implications in the bottom nepheloid layer. A case of study of the coastal zone off the Rhone River (France). *Deep-Sea Res II* 44(3/4):551–575
- Naudin JJ, Cauwet G, Chretiennot-Dinet MJ, Deniaux B, Devenon JL, Pauc H (1997) River discharge and wind influence upon particulate transfer at the land-ocean interaction: case study of the Rhone River plume. *Estuarine Coastal Shelf Sci* 45:303–316
- Naudin JJ, Cauwet G, Fajon C, Oriol L, Terzic S, Devenon JL, Broche P (2001) Effect of mixing on microbial communities in the Rhone river plume. *J Mar Systems* 28:203–227
- Neukermans G, Loisel H, Mériaux X, Astoreca R, McKee D (2012) In situ variability of mass-specific beam attenuation and backscattering of marine particles with respects to particle size, density and composition. *Limnol Oceanogr* 57(1):124–144. doi:10.4319/lo.2011.57.1.0124
- Ouillon S (2003) An inversion method for reflectance in stratified turbid waters. *Int J Remote Sensing* 24(3):535–558
- Ouillon S, Forget P, Froidefond JM, Naudin JJ (1997) Estimating suspended matter concentrations from SPOT data and from field measurements in the Rhône river plume. *MTS J* 31(2):15–20
- Pont D, Simonnet J, Walter V (2002) Medium-term changes in suspended sediment delivery to the ocean: consequences of catchment heterogeneity and river management (Rhône River, France). *Estuarine Coastal Shelf Sci* 54:1–18
- Ras J, Uitz J, Claustre H (2008) Spatial variability of phytoplankton pigment distributions in the subtropical South Pacific Ocean: comparison between in situ and modeled data. *Biogeosciences* 5:353–369
- Robinson AR, Brink KH (2005) The global coastal ocean: multiscale interdisciplinary processes. Harvard University Press, Cambridge
- Stramski D, Bricaud A, Morel A (2001) Modeling the inherent optical properties of the ocean based on the detailed composition of planktonic community. *Appl Optics* 40:2929–2945
- Ulses C, Estournel C, Durrieu de Madron X, Palanques (2008) Suspended sediment transport in the Gulf of Lions (NW Mediterranean): impact of extreme storms and floods. *Cont Shelf Res* 28:2048–2070
- Van der Linde DW (1998) Protocol for determination of total suspended matter in oceans and coastal zones. Joint Research Centre, Brussels, Tech Note I.98.182
- Wheatcroft RA, Borgeld JC (2000) Oceanic flood deposits on the northern California shelf: large-scale distribution and small-scale physical properties. *Cont Shelf Res* 20:2163–2190